Nucleation and Order of a Polymer in a Confined Liquid Crystal Matrix

Lan Liu[1], Sookyung Joo[2], Xu Yang[1], Carlos J. García-Cervera[1,3], Hector D. Ceniceros[1,*]

[1] *Department of Mathematics, University of California, Santa Barbara, CA 93106, United States.*
[2] *Department of Mathematics & Statistics, Old Dominion University, Norfolk, VA 23529, United States.*
[3] *Basque Center for Applied Mathematics, Mazarredo 14, E48009 Bilbao, Basque Country, Spain.*

Abstract. We present a numerical investigation of nucleation and ordered structure formation of a flexible polymer in a nematic liquid crystal matrix confined between two parallel walls in both a 2D and a 3D channel geometry. The model is of Landau-de Gennes type for a conserved, compositional order parameter and a non-conserved, orientational tensor order parameter and allows a study at the nanoscale. The resulting system is numerically stiff, with several high order nonlinear coupled terms. This poses a significant numerical challenge that we overcome with a linearly implicit method. This investigation focuses on the effects of wall and surface anchoring on the nucleation of ordered, polymer-rich domains as well as in the selection of lamellae. In 2D, we find that chains of polymer-rich droplets nucleate, starting at the walls and aligned with them, and continue to form until they fill up much of the channel. Without orientational defects observed in the liquid crystal-rich phase, the droplets eventually coalesce, coarsen, and the linear chain order is destroyed. In 3D, the polymer nucleates into layers of cylindrical structures, instead of droplets, whose principal axis is oriented with the wall anchoring angle. We also find that when the liquid crystal component is initially in isotropic state, stable equilibrium lamellae can be obtained for both homeotropic and planar surface anchoring conditions, in 2D and 3D.

AMS subject classifications: 76A15, 35Q99

Key words: nucleation, ordered structure, Laudau-de Gennes, nematic liquid crystal, anchoring

---

Corresponding author. Email addresses: `lanliu@ucsb.edu` (L. Liu), `xuyang@math.ucsb.edu` (X. Yang), `sjoo@odu.edu` (S. Joo), `cgarcia@math.ucsb.edu` (C.J. García-Cervera), `ceniceros@ucsb.edu` (H.D. Ceniceros)

1 Introduction

Nematic liquid crystals are an intermediate phase of matter between the commonly observed solid and liquid states of matter [1]. In recent years, phase separation of a mixture of a nematic liquid crystal (LC) and an isotropic material such as a flexible polymer has attracted increased attention as this system offers a significant potential for applications [2–15]. After a temperature quench, the phase separation process proceeds through a fast initial formation (nucleation) of small particles, a subsequent slow growth, and coarsening until a steady state is reached [16,17]. For example, polymer-dispersed liquid crystals (PDLCs), which consist of an isotropic polymer matrix and a LC droplet phase are being used in switchable windows, displays, spatial light modulators, tunable filters, and other devices [7,18,19]. There have also been recent applications of PDLCs involving phase separation induced from rapid temperature quenching [20–28].

In order to better control and design the properties of these materials, it is crucial to understand the phase separation process and the ultimate morphologies. Due to the complexity of physical models used for phase separation, it is necessary to resort to numerical simulations for a systematic study. In this work, we report on a computational investigation of the nucleation mechanism of a polymer in a LC continuous phase in a 2D and a 3D channel with the following setup: the polymer-LC system is confined between two parallel walls which provide strong planar long-range wall anchoring, and rapid temperature quenching induces the nucleation of the minority phase.

In earlier studies, a phase field model with a vector order parameter n has been widely employed for these binary systems [2,3,29]. However, a vector does not have head-to-tail symmetry and is incapable to learn biaxial states nor capture line defects. To better describe the domain anisotropy, our framework employs the more comprehensive Landau-de Gennes model which applies a tensor order parameter Q to describe the orientation of the rigid-rod like liquid crystal molecules. The free energy of the system is then formulated with the conserved volume fraction of the species and the non-conserved tensor order parameter. The evolution of the system is governed by the coupled time-dependent Ginzburg-Landau equations (model C) [30, 31]. Similar models have been extensively used in phase separation with some degree of simplification [4–6, 12–15]. To the best of our knowledge, this is the first time the full model has been utilized to learn the phase separation in confined geometries for a 3D geometry.

The Landau-de Gennes model poses significant numerical challenges. It is a large, highly nonlinear, and coupled system with up to fourth order derivative terms in the compositional order parameter ϕ, and several second order terms in the tensor order parameter Q equations. This makes the time integration markedly stiff. In addition, Q must remain traceless at each time step, and to preserve the integral of ϕ and be consistent with the variation of the free energy, a nontrivial boundary condition has to be enforced at the walls. We overcome these computational challenges with the implementation of a linearly implicit method, a strict enforcement of the traceless condition, and an extrapolated boundary condition.

We find that the nematic component and wall anchoring have profound effect on structure formation. By varying thermotropic parameters which control the isotropic to nematic transition temperature of the LC in the presence of the polymer component, we are able to select the initial state of the LC to be nematic or isotropic and this leads to two strikingly different results. In one case, small polymer-rich droplets nucleate in a LC continuous phase and form ordered chain structures, layer by layer, in the early phase separation process in 2D, and cylindrical chain structures in 3D. The colloidal dispersions and emulsions of this type have attracted considerable attention because of the striking self-assembly morphologies [32–38], which offer great potential applications [39,40]. The colloidal particles disturb the orientational field and produce defects which stabilize droplet chain structures. Theoretical [41] and numerical [42] studies on nematic liquid crystal colloids indicate that a dipole orientational defect produced in between the droplets stabilize the chain. With the Landau-de Gennes model we are able to observe these chain structures, starting at the walls and propagating into the interior, during a first stage in the phase separation process. However, as we show with one example, dipole defects are not preserved in the Landau-de Gennes model and split into $-1/2$ point defects. As a result, without the presence of dipole defects, the chain order is ultimately destroyed by coarsening and coalescence. In the second case, in which we consider a mixture in which the LC is initially in isotropic state, we find that the system phase separates into stable equilibrium lamellae, with alternating polymer-rich and LC-rich layers filling the entire region for both the 2D and 3D channel and when either homeotropic or planar surface anchoring conditions prevail.

The remainder of the paper is organized as follows: Section 2 describes the Landau-de Gennes theory to model the free energy, the kinetic equation and the boundary conditions. Section 3 discusses the numerical method employed to solve the differential equations. Section 4 presents a summary of numerical results for simulations in 2D and 3D channels. Concluding remarks are given in Section 5.

2 Landau-de Gennes Model

2.1 Landau-de Gennes Free Energy

We consider a binary mixture of an isotropic material, such as a flexible polymer, and nematic liquid crystal contained between two parallel walls. To study the nucleation of the polymer induced from rapid temperature quenching, we consider the thermodynamic behavior of our system, and the Landau-de Gennes theory is applied, which involves a tensor order parameter Q that is capable of describing the biaxial states. In contrast, the other commonly used continuum theory for nematic liquid crystals is the Oseen-Frank model, which relies only on the director field n but fails to capture disclination line defects and biaxial states [43].

The tensor order parameter Q in the Landau-de Gennes theory is a symmetric, traceless 3 by 3 matrix which describes the orientational ordering of a liquid crystal. The

eigenvectors of Q represent the average directions of alignment of the molecules, and the associated eigenvalues measure the degree of alignment along these directions. The generic biaxial state corresponds to a Q tensor with three distinct eigenvalues. In contrast, uniaxial states appear when two of the eigenvalues are the same and can be simplified into the form [1]:

$$Q = S(\boldsymbol{n} \otimes \boldsymbol{n}) - \frac{1}{3} S \boldsymbol{I}, \quad S \in \mathbb{R}, \, n \in \mathbb{S}^2, \tag{2.1}$$

where $S \in [-\frac{1}{2}, 1]$ represents the degree of orientational ordering and the unit vector $\boldsymbol{n}$ indicates the average direction of the uniaxial rod-like liquid crystal molecules. The biaxiality parameter in the liquid crystal literature is usually defined as [44,45]:

$$\beta(Q) = 1 - 6 \frac{(tr(Q^3))^2}{(tr(Q^2))^3}, \tag{2.2}$$

where $\beta(Q) \in [0,1]$, and $\beta(Q) = 0$ stands for the uniaxial case.

The system containing a flexible polymer and a nematic liquid crystal can be described with the tensor order parameter Q and a phase field $\phi \in [0,1]$ that represents the local volume fraction of the flexible isotropic polymer in the binary mixture. Assuming the incompressibility of the system, the local volume fraction of the nematic liquid crystal is thus $1 - \phi$. Therefore, the pure, bulk phases are identified with $\phi = 0$ and $\phi = 1$ for the nematic liquid crystal and the isotropic fluid, respectively.

The free energy density $f(Q,\phi)$ of the system consists of two parts: the Flory-Huggins free energy [46, 47], which governs phase separation, and the Laudau-de Gennes free energy, which governs the nematic component. More specifically, four terms appear: a mixing energy density f_{mix}, an orientational distortion energy density of the nematic, f_{ela}, a thermotropic energy density that describes the preferred phase of the nematic, f_{ther}, and the anchoring energy density of the nematic molecules at interfaces, f_{anc}:

$$f(Q,\phi) = f_{mix} + (1-\phi)(f_{ther} + f_{anc} + f_{ela}), \tag{2.3}$$

where

$$f_{mix}(\phi) = \frac{\lambda_c}{2} \left[|\nabla \phi|^2 + \frac{\beta \phi \ln \phi + (1-\phi) \ln(1-\phi) + \frac{g_0}{T} \phi(1-\phi)}{2\epsilon_c^2} \right], \tag{2.4}$$

$$f_{ther}(Q,\phi) = \frac{A_c(\phi)}{2} Tr Q^2 + \frac{B_c}{3} Tr Q^3 + \frac{C_c}{4} (Tr Q^2)^2, \tag{2.5}$$

$$f_{ela}(Q) = \frac{K_c}{2} (\nabla_\gamma Q_{\alpha\beta})(\nabla_\gamma Q_{\alpha\beta}), \tag{2.6}$$

$$f_{anc}(Q,\phi) = \frac{W_c}{2}(\nabla_\alpha \phi)(\nabla_\beta \phi)Q_{\alpha\beta}. \tag{2.7}$$

In (2.4), λ_c is the mixing energy strength with units of J/m, ϵ_c is the capillary width with units of length, and β denotes the molecular volume ratio of the liquid crystal and isotropic fluid molecules. The coefficient $\frac{g_0}{T}$ is the Flory-Huggins interaction parameter related to the van der Waals interactions between unlike molecular species, where T is the temperature.

In (2.5), $A_c(\phi)$, B_c, C_c are temperatures and material dependent with units of Jm^{-3}. Usually we assume B_c and C_c are independent of temperature while $A_c(\phi) = a_c(T - T_{NI}^*(\phi))$, where $T_{NI}^*(\phi)$ is the super-cooling temperature at which the isotropic state loses stability. Here we assume $T_{NI}^* = T_c - d\phi$, where T_c is super-cooling temperature in the absence of isotropic fluid, and the relationship implies that nematic ordering is disturbed by the existence of isotropic phase so that the transition temperature is a decreasing function of ϕ [4, 48]. The set of Q that minimizes the potential f_{ther} obviously plays a crucial role, which determines the equilibrium state of the liquid crystal under different temperatures. It can be found as uniaxial $Q = S_{eq}(\mathbf{n} \otimes \mathbf{n} - \frac{1}{3}\mathbf{I})$ with equilibrium scalar order parameter as follows:

$$S_{eq} = \begin{cases} 0 & T > T_{NI}, \\ \frac{1}{4C_c}(-B_c + \sqrt{B_c^2 - 24A_c(\phi)C_c}) & T < T_{NI}, \end{cases} \tag{2.8}$$

where $T_{NI} = T_{NI}^*(\phi) + \dfrac{B_c^2}{27a_cC_c}$ is the isotropic-nematic transition temperature.

In (2.6), the elastic deformation can always be decomposed in three basic deformation modes, splay, twist and bend [1]. The common formulation of the distortional free energy with respect to Q reads [49]:

$$f_{ela}(Q) = \frac{1}{2}L_1 \frac{\partial Q_{ij}}{\partial x_k}\frac{\partial Q_{ij}}{\partial x_k} + \frac{1}{2}L_2 \frac{\partial Q_{ij}}{\partial x_k}\frac{\partial Q_{ik}}{\partial x_j} + \frac{1}{2}L_3 \frac{\partial Q_{ij}}{\partial x_j}\frac{\partial Q_{ik}}{\partial x_k} + \frac{1}{2}L_4 Q_{ij}\frac{\partial Q_{kl}}{\partial x_i}\frac{\partial Q_{kl}}{\partial x_j}. \tag{2.9}$$

With one-constant approximation, we assume $L_1 = K_c$, $L_2 = L_3 = L_4 = 0$, and K_c denotes the elastic energy strength of units J/m.

Lastly, in (2.7), W_c is the surface anchoring energy strength given in J/m. Note that as $W_c < 0$, the homeotropic anchoring is favorable for which the molecules tend to align perpendicular to the interface, in contrast, as $W_c > 0$, the planar anchoring is preferred with tangential alignment.

As mentioned by Ravnik et al. [42], the ratio of the thermotropic energy f_{ther} and distortional energy f_{ela} introduces a characteristic length scale ξ_N, which is referred to as nematic correlation length. It determines the spatial scale for the variation of the nematic order. Its role in nematic is most profound in defects as it roughly determines its size. We

will use ξ_N to control the mesh resolution in the later numerical calculations. A simple calculation as in [42] will yield

$$\xi_N = \sqrt{\frac{K_c}{a_c(T-T^*_{NI})+2/3B_cS_{eq}+2C_cS^2_{eq}}}. \tag{2.10}$$

The total free energy is now given by

$$F = \int_\Omega f(\phi,Q)dV, \tag{2.11}$$

where $\Omega = [0,L_{xc}]\times[0,L_{yc}]$ for a 2D channel and $\Omega = [0,L_{xc}]\times[0,L_{yc}]\times[0,L_{zc}]$ for a 3D channel.

2.2 Kinetic Equation and Boundary Conditions

The evolution of the conserved volume fraction ϕ and non-conserved orientational order parameter Q are governed by the coupled time-dependent Ginzburg-Landau equations (model C) which ensures the monotonic decrease of the total energy:

$$\frac{\partial \phi}{\partial t} = \nabla \cdot \left(M_\phi \nabla \frac{\delta F}{\delta \phi} \right) + \eta,$$

$$\frac{\partial Q_{\alpha\beta}}{\partial t} = -M_Q \frac{\delta F}{\delta Q_{\alpha\beta}} + \eta_{\alpha\beta} + \lambda\delta_{\alpha\beta}, \tag{2.12}$$

where M_ϕ and M_Q are the mobility coefficients that depend on the molecular weights of isotropic and liquid crystal molecules as well as the local composition density ϕ and orientational order parameter Q. They are assumed to be constants in the simulation as employed by Motoyama et al. [4]. Here $\delta_{\alpha\beta}$ stands for the Kronecker delta. The thermal noise η and $\eta_{\alpha\beta}$ are neglected, and λ is determined by the traceless condition $TrQ=0$. We note that a Lagrangian multiplier for the symmetry constraint, $Q_{ij}=Q_{ji}$, is omitted here because non-symmetrical terms in (2.9) were assumed to be zero. The system (2.12) comprises six coupled nonlinear parabolic partial differential equations.

The system can be nondimensionalized by selected characteristic length and energy scales L_c and E_c. Then, the free energy parameters are made dimensionless as $\lambda = \lambda_c L_c/E_c, \epsilon = \epsilon_c/L_c, g = g_0/T, W = W_c L_c/E_c, K = K_c L_c/E_c, A = A_c L_c^3/E_c, B = B_c L_c^3/E_c, C = C_c L_c^3/E_c, L_x = L_{xc}/L_c, L_y = L_{yc}/L_c, L_z = L_{zc}/L_c$.

Computing the variational derivative of (2.12), we generate the coupled system of the

equations that simulates the phase separation of the mixture:

$$\frac{1}{M_Q}\frac{\partial Q_{\alpha\beta}}{\partial t} = K\nabla_\gamma[(1-\phi)\nabla_\gamma Q_{\alpha\beta}] - (1-\phi)\Big[\frac{W}{2}(\nabla_\alpha\phi)(\nabla_\beta\phi) - \frac{W}{6}|\nabla\phi|^2\delta_{\alpha\beta}$$

$$+ \{A+C(TrQ^2)\}Q_{\alpha\beta} + B(Q^2)_{\alpha\beta} - \frac{B}{3}TrQ^2\delta_{\alpha\beta}\Big],$$

$$\frac{1}{M_\phi}\frac{\partial\phi}{\partial t} = \nabla\cdot\nabla\Big[\lambda\Big(-\nabla^2\phi + \frac{\beta\ln(\phi) - \ln(1-\phi) - 2g\phi}{4\epsilon^2}\Big) + (1-\phi)\frac{ad}{2}TrQ^2$$

$$-W\nabla_\alpha\{(1-\phi)(\nabla_\beta\phi)Q_{\alpha\beta}\} - \frac{K}{2}(\nabla_\gamma Q_{\alpha\beta})(\nabla_\gamma Q_{\alpha\beta})$$

$$-\frac{W}{2}(\nabla_\alpha\phi)(\nabla_\beta\phi)Q_{\alpha\beta} - \frac{A}{2}TrQ^2 - \frac{B}{3}TrQ^3 - \frac{C}{4}(TrQ^2)^2\Big].$$

(2.13)

The terms $-\frac{W}{6}|\nabla\phi|^2\delta_{\alpha\beta}$ and $-\frac{B}{3}TrQ^2\delta_{\alpha\beta}$ are added to preserve the traceless property of Q [4,6]. The following boundary conditions are required to be satisfied:

$$\int_{\partial\Omega} KP_{\alpha\beta}(1-\phi)\frac{\partial Q_{\alpha\beta}}{\partial\nu}ds = 0,$$

(2.14)

$$\int_{\partial\Omega} \psi\Big[\frac{\partial\phi}{\partial\nu} + W(1-\phi)\nabla\phi\cdot Q^T\cdot\nu\Big]ds = 0,$$

(2.15)

where ν denotes the outward normal vector to $\partial\Omega$, and $P_{\alpha\beta}$ and ψ are the testing function of $Q_{\alpha\beta}$ and ϕ, respectively.

We consider a rectangular domain that the polymer-LC system is confined in between the two walls and periodic boundary conditions are imposed in the parallel-wall direction, which ensure (2.14) and (2.15) to be hold along the horizontal boundaries. For the Y boundaries, the walls are usually glass slides that being coated and rubbed to obtain uniform long-range anchoring, which makes the molecules homogeneously aligned parallel to the walls. This implies the prescribed boundary value for Q, and (2.14) is satisfied with test function $P_{\alpha\beta}$ which vanishes at the walls. More specifically,

$$Q\Big|_{y=0,L_y} = Q^s = S_{eq}(\tau\otimes\tau - \frac{1}{3}I),$$

(2.16)

where S_{eq} is determined by (2.8), and τ is the in plane director field along the walls whose direction is determined by how the glass slides are rubbed. It provides the planar long-range wall anchoring for our system.

Now we explore the boundary condition of ϕ at the wall to satisfy (2.15). Denote the unit normal vector of the walls as ν, and a unit vector τ representing the planar wall anchoring, therefore, $\tau\cdot\nu = 0$, which implies:

$$Q\cdot\nu = S(\tau\otimes\tau - \frac{1}{3}I)\cdot\nu = -\frac{1}{3}S\nu,$$

(2.17)

apply to (2.15),

$$\frac{\partial \phi}{\partial \boldsymbol{\nu}} + W(1-\phi)\nabla\phi \cdot Q^T \cdot \boldsymbol{\nu} = \frac{\partial \phi}{\partial \boldsymbol{\nu}} - \frac{W}{3}(1-\phi)S\nabla\phi \cdot \boldsymbol{\nu} = \frac{\partial \phi}{\partial \boldsymbol{\nu}}\left(1 - \frac{W}{3}S + \frac{W}{3}\phi S\right) = 0, \quad (2.18)$$

which implies,

$$\left.\frac{\partial \phi}{\partial \boldsymbol{\nu}}\right|_{y=0,L_y} = 0. \tag{2.19}$$

The Neumann boundary condition at the walls is sufficient for ϕ to satisfy (2.15). It is also worthwhile noting that the differential equation of ϕ is 4-th order in (2.13), and another boundary condition for ϕ is required. It is derived from the fact that ϕ is a conserved quantity, i.e.

$$\frac{d}{dt}\int_\Omega \phi dV = \int_\Omega \nabla\cdot(M_\phi \nabla\frac{\delta F}{\delta \phi})dV = \int_{\partial\Omega} M_\phi \frac{\partial}{\partial \boldsymbol{\nu}}(\frac{\delta F}{\delta \phi})ds = 0. \tag{2.20}$$

Along parallel-wall direction, this holds because of the periodic boundary condition. Along Y boundary, we want to set $\left.\dfrac{\partial}{\partial \boldsymbol{\nu}}\left(\dfrac{\delta F}{\delta \phi}\right)\right|_{y=0,L_y} = 0$. More explicitly,

$$\left.\frac{\partial(\lambda(\nabla^2\phi))}{\partial \boldsymbol{\nu}}\right|_{y=0,L_y} = \frac{\partial}{\partial \boldsymbol{\nu}}\left[\lambda(\frac{\beta\ln(\phi)-\ln(1-\phi)-2g\phi}{4\epsilon^2}) + (1-\phi)\frac{ad}{2}TrQ^2\right.$$

$$-W\nabla_\alpha\{(1-\phi)(\nabla_\beta\phi)Q_{\alpha\beta}\} - \frac{K}{2}(\nabla_\gamma Q_{\alpha\beta})(\nabla_\gamma Q_{\alpha\beta})$$

$$\left.-\frac{W}{2}(\nabla_\alpha\phi)(\nabla_\beta\phi)Q_{\alpha\beta} - \frac{A}{2}TrQ^2 - \frac{B}{3}TrQ^3 - \frac{C}{4}(TrQ^2)^2)\right]\Bigg|_{y=0,L_y}.$$

$$\tag{2.21}$$

3 Numerical Method

At each time step, we need to solve five second order partial differential equations (PDEs) for $Q_{\alpha\beta}$ and one fourth order PDE for ϕ. We enforce strictly the traceless requirement for Q by determining Q_{33} directly from this condition. This coupled system is numerically stiff due to the presence of many high order spatial derivatives. In addition, there are two distinctly different time scales, a fast one associated with an initial fast phase separation and a slow one in which domain coarsening takes place. In order to relax the numerical stiffness, we employ a semi-implicit method in which we identify the linearly dominant terms at small scales and discretize these implicitly while treating the remaining nonlinear terms explicitly.

For 2D channel, we assume there are no gradients in the z direction, i.e. $\nabla_z f = 0$ for any of the relevant functions f. The time discretized form of (2.13) can be written as follows:

$$\frac{1}{M_Q}\frac{Q_{\alpha\beta}^{j+1}-Q_{\alpha\beta}^{j}}{\Delta t}=\mu_1(\Delta Q_{\alpha\beta})^{j+1}+g(\phi^j,Q_{\alpha\beta}^j),\tag{3.1}$$

$$\frac{1}{M_\phi}\frac{\phi^{j+1}-\phi^j}{\Delta t}=\nabla\cdot\nabla(-\lambda(\Delta\phi)^{j+1}+\mu_2\phi^{j+1}+h(\phi^j,Q_{\alpha\beta}^j)),\tag{3.2}$$

where

$$\begin{aligned}g(\phi,Q_{\alpha\beta})=&(K(1-\phi)-\mu_1)\Delta Q_{\alpha\beta}-K\nabla\phi\cdot\nabla Q_{\alpha\beta}-(1-\phi)[\frac{W}{2}(\nabla_\alpha\phi)(\nabla_\beta\phi)\\&-\frac{W}{6}|\nabla\phi|^2\delta_{\alpha\beta}+\{A+C(TrQ^2)\}Q_{\alpha\beta}+B(Q^2)_{\alpha\beta}-\frac{B}{3}TrQ^2\delta_{\alpha\beta}],\end{aligned}\tag{3.3}$$

$$\begin{aligned}h(\phi,Q_{\alpha\beta})=&-\mu_2\phi+\lambda(\frac{\beta\ln(\phi)-\ln(1-\phi)-2g\phi}{2\epsilon^2})+\frac{ad}{2}(1-\phi)TrQ^2\\&-\frac{K}{2}(\nabla_\gamma Q_{\alpha\beta})(\nabla_\gamma Q_{\alpha\beta})-W\nabla_\alpha\{(1-\phi)(\nabla_\beta\phi)Q_{\alpha\beta}\}\\&-\frac{W}{2}(\nabla_\alpha\phi)(\nabla_\beta\phi)Q_{\alpha\beta}-\frac{A}{2}TrQ^2-\frac{B}{3}TrQ^3-\frac{C}{4}(TrQ^2)^2.\end{aligned}\tag{3.4}$$

Here, μ_1 and μ_2 are numerical parameters introduced to relax the timestep stability constraint [50].

$$\mu_1=\frac{\max(K(1-\phi))}{2},\tag{3.5}$$

$$\mu_2=\max\left|\frac{d}{d\phi}\lambda(\frac{\beta\ln(\phi)-\ln(1-\phi)-2g\phi}{2\epsilon^2})\right|.\tag{3.6}$$

These equations are solved on a rectangular domain with periodic boundary condition along the horizontal direction. Thus, we perform a discrete Fourier transform along the x and z directions to obtain a linear system along the y direction.

At the walls we have a Dirichlet boundary condition for Q (2.16) and Neumann boundary conditions for ϕ and for the Laplacian of ϕ, (2.19) and (2.21), respectively. The latter involves derivatives of Q and since these are not specified at the boundary, condition (2.21) represents a notable challenge. Other numerical investigations have avoided this problem by opting to use instead the homogeneous Neumann boundary condition.

We find that the boundary conditions for ϕ can be expressed in the following form:

$$\begin{aligned}&\frac{\partial\phi}{\partial\nu}=0,\\&\frac{\partial^3\phi}{\partial\nu^3}=\frac{1}{\lambda}\frac{\partial h}{\partial\nu}=0,\end{aligned}\tag{3.7}$$

which makes its enforcement more tractable. Specifically, to obtain $h(\phi,Q)$ at the walls ($n=1$ and $n=N$) we extrapolate $\nabla_\nu Q_{\alpha\beta}$ from the interior values. The algorithm flow is shown in Fig. 1.
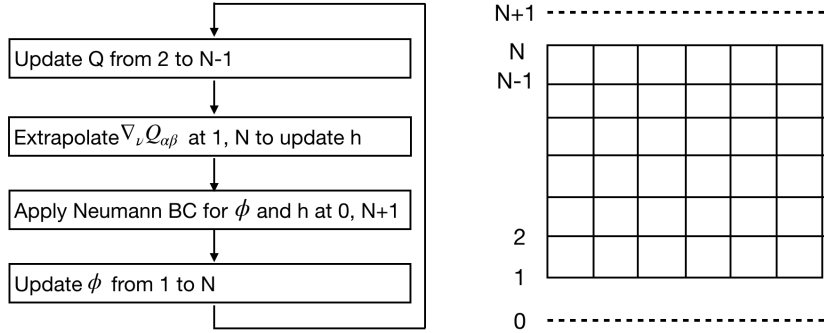
Figure 1: Algorithm flow of the coupled system. The dashed line at 0 and $N+1$ are ghost points induced for ϕ and h, whose values are found by Neumann boundary condition.

4 Numerical Results and Discussion

We present next our numerical results of ordering and structure formation of an isotropic material, such as a flexible polymer, nucleating in a liquid crystal (LC) continuous phase for both a 2D and a 3D channel. The polymer-LC system is confined between two parallel walls and periodic boundary conditions are imposed in the parallel-wall direction. We are particularly concerned with the interplay of phase separation and nematic ordering induced by wall anchoring so we impose planar anchoring at the walls (i.e. at the walls the nematic alignment is parallel to them) and examine both homeotropic (normal to the walls) and planar anchoring at the polymer-LC surfaces.

In all the simulations here reported, the free energy decreased monotonically per step and the total polymer volume fraction was preserved accurately with a 10^{-13} variation after 10^4 steps. These quantities were approximated with the composite trapezoidal rule.

4.1 Parameters

There is a large number of parameters in the Landau-de Gennes model. We have chosen these parameters to approximate those of a 5CB nematic liquid crystal [42]. Their values and the numerical mesh sizes are provided in Table 1. The quenching temperature, and initial composition were selected so that some phase separation (nucleation) takes place before there is any significant orientational order away from the walls. Two sets of thermotropic energy parameters (a, B, and C) were considered (labeled Set 1 and Set 2 in Table 1) to obtain an initially nematic and an isotropic state of the LC component as determined by S_{eq}, which is evaluated using (2.8) with $\phi = 0.4$ as the initial, mean polymer concentration. The two values of S_{eq} in Table 1 correspond to a weakly nematic initial state of the LC for Set 1 and an isotropic state for Set 2.

The correlation length ζ_N, which gives a measure of the orientational defect size if

there is any, was computed using (2.10). Consequently, to adequately resolve such small length scale we take the uniform mesh size to be $\Delta x_c = \Delta y_c = 10nm$. The time step size is $\Delta t = 0.1$ and remains constant throughout all simulations. For 2D experiments, the rectangular domain size is set to be $L_{xc} = 2.56\mu m$ and $L_{yc} = 2.56\mu m$. For 3D case, $L_{xc} = 1.28\mu m$, $L_{yc} = 1\mu m$, and $L_{zc} = 1.28\mu m$. In both instances, the normal-wall direction is y.

Parameters	Set 1	Set 2
λ_c	$4 \times 10^{-11} J/m$	*
K_c	$4 \times 10^{-11} J/m$	*
W_c	$-1 \times 10^{-10} J/m$	*
a_c	$0.553 \times 10^5 J/m^3 K$	$8 \times 10^5 J/m^3 K$
B_c	$-0.7155 \times 10^6 J/m^3$	$-0.1 \times 10^6 J/m^3$
C_c	$0.8758 \times 10^6 J/m^3$	$1.6 \times 10^6 J/m^3$
M_Q	$10^{-20} m^3/J\Delta t$	*
M_ϕ	$10^{-4} m^3/J\Delta t$	*
β	1	*
g_0	2.8K	*
T	1.3K	*
T_c	2K	*
d	2K	*
ϵ_c	50nm	*
S_{eq}	0.384	0
ξ_N	22.29nm	85.05nm
Δx_c	10nm	*
Δy_c	10nm	*
Δt	0.1	*

Table 1: Two sets of parameters used for numerical simulations. Set 1 corresponds roughly to 5CB nematic liquid crystal [42], and $*$ in set 2 takes the same value as in set 1. The temperature related parameters are taken from [4].

As mentioned in Section 2, the parameters are nondimensionalized by choosing a characteristic length scale L_c and a characteristic energy scale E_c. We take $L_c = 1\mu m$ and $E_c = 1 \times 10^{-14} J$.

4.2 Initial Condition

In all the simulations we start with an initial state defined by a small perturbation of a uniform mixture, where the dominant phase is the nematic crystal ($\phi < \frac{1}{2}$),

$$\phi_0 = 0.4 + \gamma. \tag{4.1}$$

Here γ is a uniformly distributed random number in $(-0.001, 0.001)$. The initial director field n is taken to be a random unit vector.

4.3 Chain Structure Order

The experimental results of Loudet, Barois, and Poulin [32] show spectacularly that a polymer phase can nucleate in a confined nematic LC matrix to form highly ordered droplet chains whose orientation can be controlled by wall anchoring. We examine next to which extent this fascinating phenomenon can be captured by the Landau-de Gennes model.

We consider a relatively shallow quench (T=1.3) so that some phase separation occurs prior to when the orientational order becomes significant. The surface anchoring is homeotropic, i.e. the preferential nematic orientation at the polymer-LC interfaces is normal to those surfaces. After nondimensionalization, the values of the relevant parameters are $a = 5.528$, $B = -71.55$, and $C = 87.58$ for the thermotropic energy and $W = -0.01$, $K = 0.004$, and $\lambda = 0.004$ for the anchoring strength, the elastic constant, and the mixing energy strength, respectively.

Figure 2 displays a series of snapshots of the phase separation process in the 2D channel. The polymer-rich phase is shown in blue and the LC-rich phase in red. A subsampled, in-plane component of the director field is also displayed. In the early stages of the spinodal decomposition [Fig. 2(a)], a row of polymer-rich droplets is nucleated adjacent to each wall in two corresponding LC-rich layers. The wall anchoring induces an orientational order that quickly propagates from the walls inward, toward the channel center, and produces a director field that is nearly horizontal in about 2/3 of the domain. LC-rich layers immediately next to the walls have also been observed in the simulations by Xia *et al.* [6] for a similar system but with free wall anchoring (i.e. no preferred nematic orientation enforced at the walls) and with an affinity wall potential. Here, however, the LC-layers are induced by the planar wall anchoring, which has a dramatic long range effect as Fig. 2(b) shows; the director field is horizontal at the domain center and more rows of polymer-rich droplets have formed. In contrast, in a typical spinodal decomposition of a binary mixture with a dominant component as modelled by the Cahn-Hilliard equation, the minority phase starts to nucleate throughout the entire domain without any ordering.

The nucleated droplets create some distortion on the orientational order induced by the walls. Note that the surface anchoring is not strong (the director field is not entirely normal to the polymer-LC surfaces). In the current model, to simulate homeotropic surface anchoring, W has to be negative and so a large $|W|$ necessitates a larger mixing energy strength λ to keep the system well-posed. As a result, when we increase both parameters we would see elongated polymer-rich domains instead of circular droplets. In other words, there is a delicate balance of wall and surface anchoring, mixing energy, orientational elasticity and thermotropic effects that comes into play within the Landau-de Gennes model to give rise to this extraordinary ordered droplet chains. As shown in

Fig. 2(c), drop coalescence takes place in the middle of the channel at a later time and the polymer-rich domains continue to coarsen [Fig. 2(d)].

In contrast to the phase separation process depicted in Fig. 2, the experiments of Loudet, Barois, and Poulin [32] show that the coarsening is arrested once the droplets reach a critical size, so that the chain structure is preserved and stable. This is explained in [32] by the presence of a dipole orientational defect between each droplet in a chain. Our numerical solution shows no indication of such orientational defects. To investigate this further, we consider a single droplet of polymer in a nematic matrix in an orientational field that approximately corresponds to a dipole. Using this as our initial condition we observe that the dipole defect splits into two $-1/2$ defects and cannot be sustained by the model as shown in Fig. 3. These two $-1/2$ defects are surrounded by biaxial region in which the order parameter has a discontinuity. Similar observations have been made for the hedgehog dipole defect [44], which was found to be unstable for large droplet radius and low temperatures with Landau-de Gennes model and forms a $-1/2$ disclination loop about the particle, which is surrounded by a region of biaxiality [44]. Therefore, in the absence of dipole orientational defects, there is no mechanism in the Landau-de Gennes model to stop the coarsening of the polymer-rich droplets and eventually the chain structure ordering is destroyed.

We now look at the same system but in a 3D channel. The relevant physical parameters and the initial condition are the same as in the 2D channel discussed above, and homeotropic surface anchoring is chosen. The wall anchoring is again planar but now we consider two different orientations: 1) aligned with the x-axis, and 2) aligned at a 45 degree angle between the x and z axes. Figure 4 displays isosurfaces of polymer volume fraction ϕ and a subsample of the director field at $t = 1100$ and $t = 3500$ for the planar wall anchoring 1) and 2). The orientational order induced by the wall anchoring and the favored homeotropic surface anchoring produce chains of elongated cylinders of polymer-rich material instead of droplets, in contrast to the 2D case. As seen in the bottom two plots in Fig. 4, wall anchoring controls the orientation of these chain structures, which now align at a 45 degree angle between the x and z axis. The nucleation of perfectly ordered layers of polymer-rich cylinders takes place, just as in the 2D counterpart, from the walls inward, until coarsening and coalescence destroy the order.

Even though homeotropic surface anchoring is more prevalent in these systems than the planar one, we consider the latter to examine its effects on the nucleated morphology. Figure 5 shows that again polymer-rich cylinders are nucleated but now the axis of these cylinders is oriented in the direction of the wall anchoring. It is important to note that just as in the 2D case, the wall anchoring quickly produces a layer of LC-rich material adjacent to the walls at which the nucleation of the first cylinder layers begins.

4.4 Lamellae Order

We consider next the same set-up as before, an initial mean polymer volume fraction of $\phi = 0.4$, but now the LC in the mixture is initially in isotropic phase. Such state is ob-
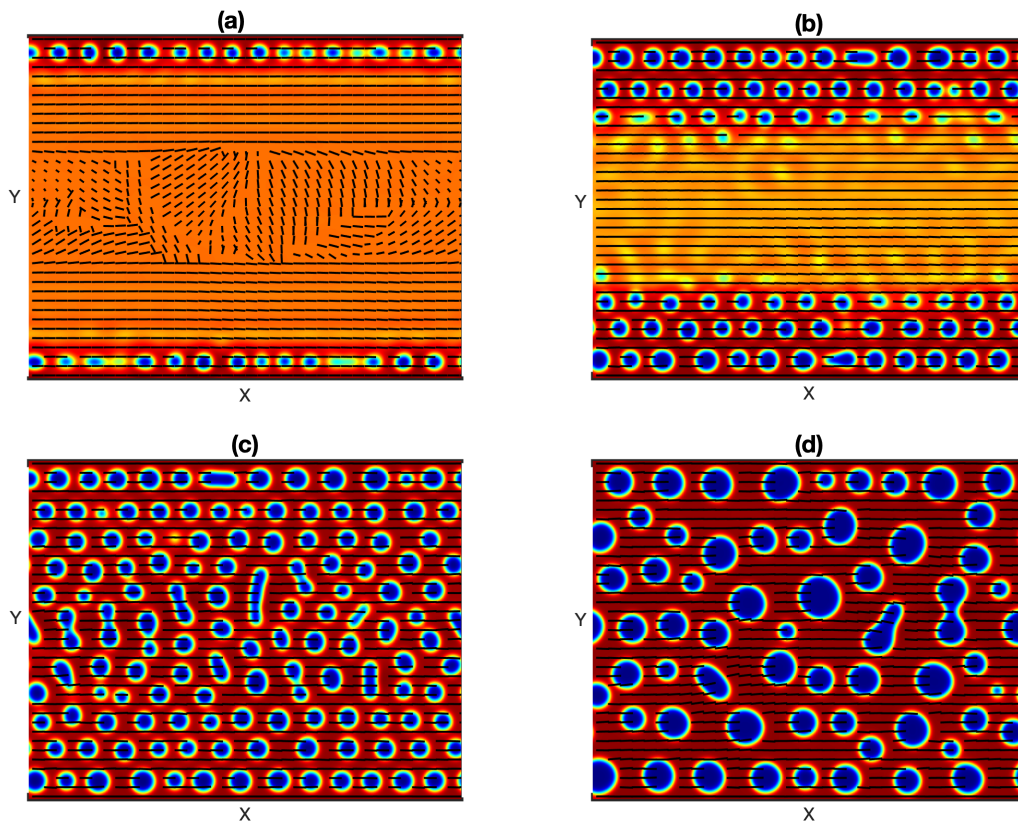
Figure 2: Time sequence of the polymer volume fraction ϕ and the subsampled director field for a polymer phase nucleating in a liquid-crystal matrix at (nondimensional times) (a) $t=1000$, (b) $t=2000$, (c) $t=3000$, and (d) $t=12000$. The thermotropic energy parameters are $a=5.528$, $B=-71.55$, $C=87.58$. LC-rich phase in red and polymer-rich phase in blue.
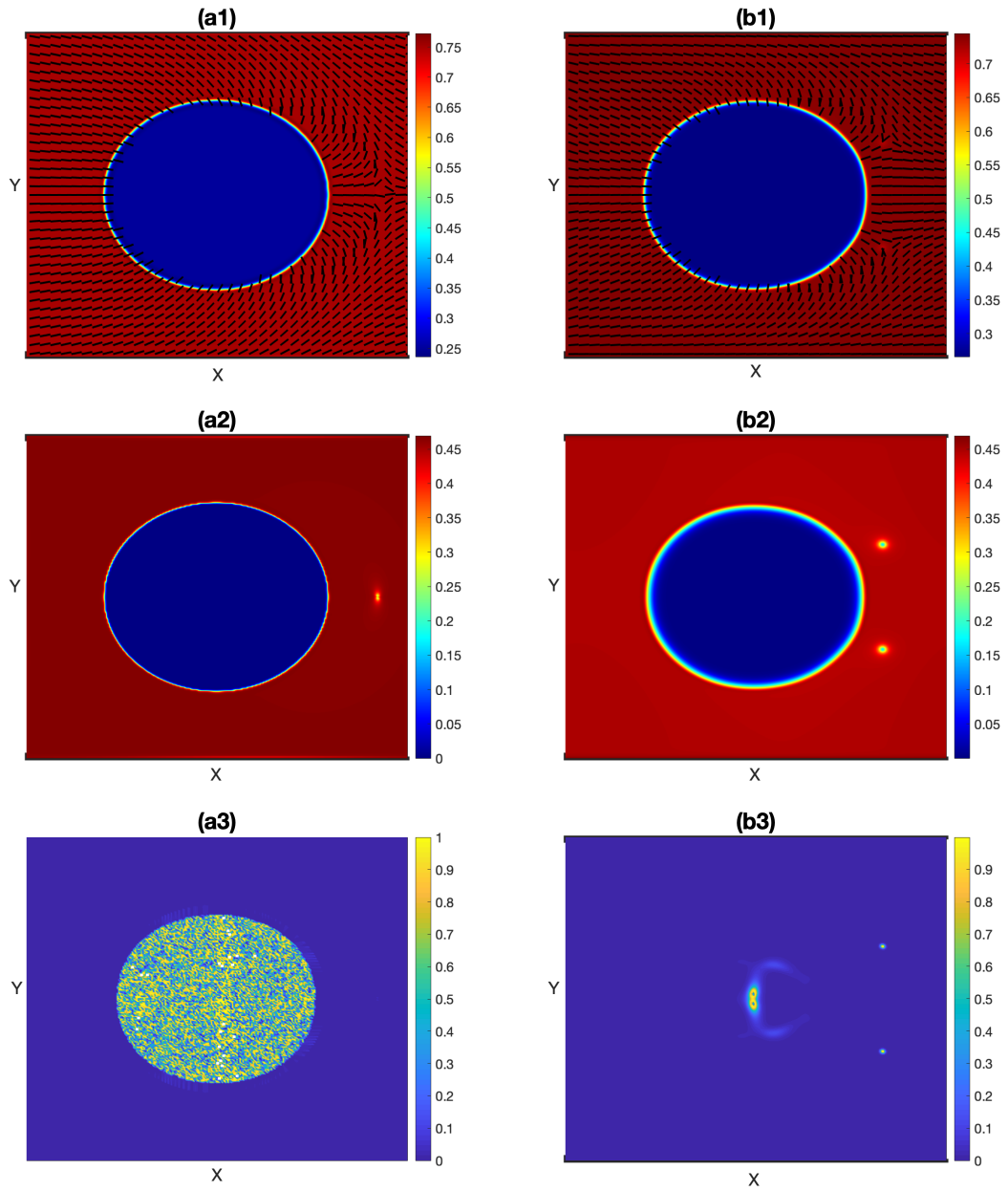
Figure 3: The top/middle/bottom plots show the polymer volume fraction ϕ with the subsampled director field $\boldsymbol{n}$, the scalar order parameter S, and the biaxiality parameter $\beta(Q)$, respectively. The (a_1), (a_2), and (a_3) plots are the initial setting at $t = 1$, which approximates a dipole point defect to the right of the droplet. The (b_1), (b_2), and (b_3) plots are at $t = 30,000$. The parameters are $a = 5.528$, $B = -71.55$, $C = 87.58$, $\lambda = 0.004$, $K = 0.002$, $W = -0.0015$. LC-rich phase in red and polymer-rich phase in blue.

(a1)

(b1)

(a2)

(b2)
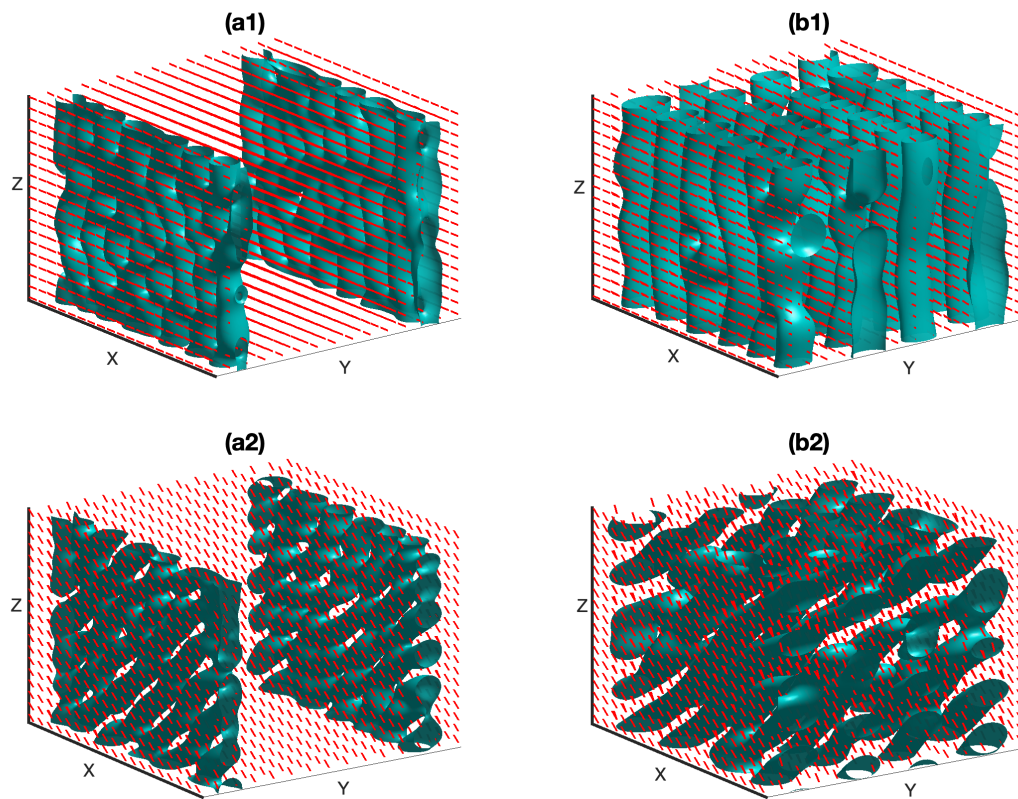
Figure 4: The top (bottom) two plots show isosurfaces and a sample of the director field at $t=1100$ (left) and $t=3500$ (right) when the wall anchoring is along the x axis (top) and at a 45 degree angle (bottom). The surface anchoring is homeotropic and the thermotropic energy parameters are $a=5.528$, $B=-71.55$, $C=87.58$.
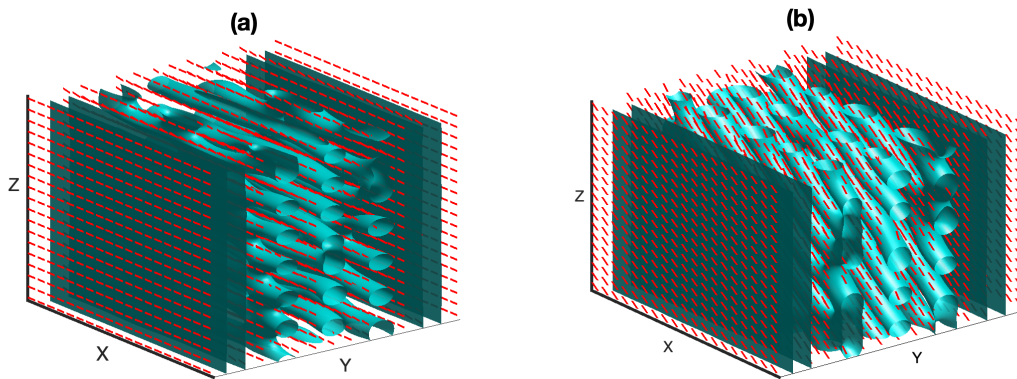
Figure 5: Isosurfaces and a sample of the director field for nucleation with planar surface anchoring and planar wall anchoring along the (a) x direction and (b) in a 45 degree angle between the x and z axes. The time step is t = 3500. The thermotropic energy parameters are $a = 5.528$, $B = -71.55$, $C = 87.58$.

tained by changing the thermotropic energy coefficients to $a = 80$, $B = -10$, $C = 160$, which with $\phi = 0.4$ give $S_{eq} = 0$. All the other parameters remain the same (Set 2 in Table 1). The wall anchoring remains planar. We consider first homeotropic surface anchoring. Figure 6 shows snapshots of the phase separation process in the 2D channel. At early times [Fig. 6(a)] a layer of LC-rich material develops adjacent to the each wall, just as in the chain structure nucleation case, but now these first LC-rich layers are accompanied by equal polymer-rich layers. As the initial isotropic binary mixture phase-separates at the walls, the strong anchoring there induces the lamellae. A similar appearance of phase-separated layers adjacent to walls has been observed in a thin film of a polymer blend [51], a diblock copolymer [52], and a polymer dispersed nematic [6] when they were confined between two walls. As Fig. 6(a) shows, these layers drastically modify the orientational field, turning it vertically aligned to comply with the homeotropic surface anchoring preference, a significant distance from the walls. This orientational distortion favors the formation of more lamellae [Fig. 6(b)], which alternate in polymer-rich and LC-reach composition, and propagate from the walls inward to fill the entire channel [Fig. 6(c)(d)]. Once this occurs the system is in equilibrium and the lamellae do not coarsen, in striking contrast to what happens in spinodal decomposition of a binary isotropic mixture (as modeled by the Cahn-Hilliard equation). Indeed, Fig. 7 shows the total energy reaches a minimum and the anchoring and elastic energies perfectly balance each other out and an equilibrium is attained.

Surface anchoring plays a crucial role in the formation of lamellae from an initially isotropic mixture such as the one just considered (parameter Set 2 in Table 1). If we choose planar surface anchoring, as shown in Fig. 8, the system phase separates into
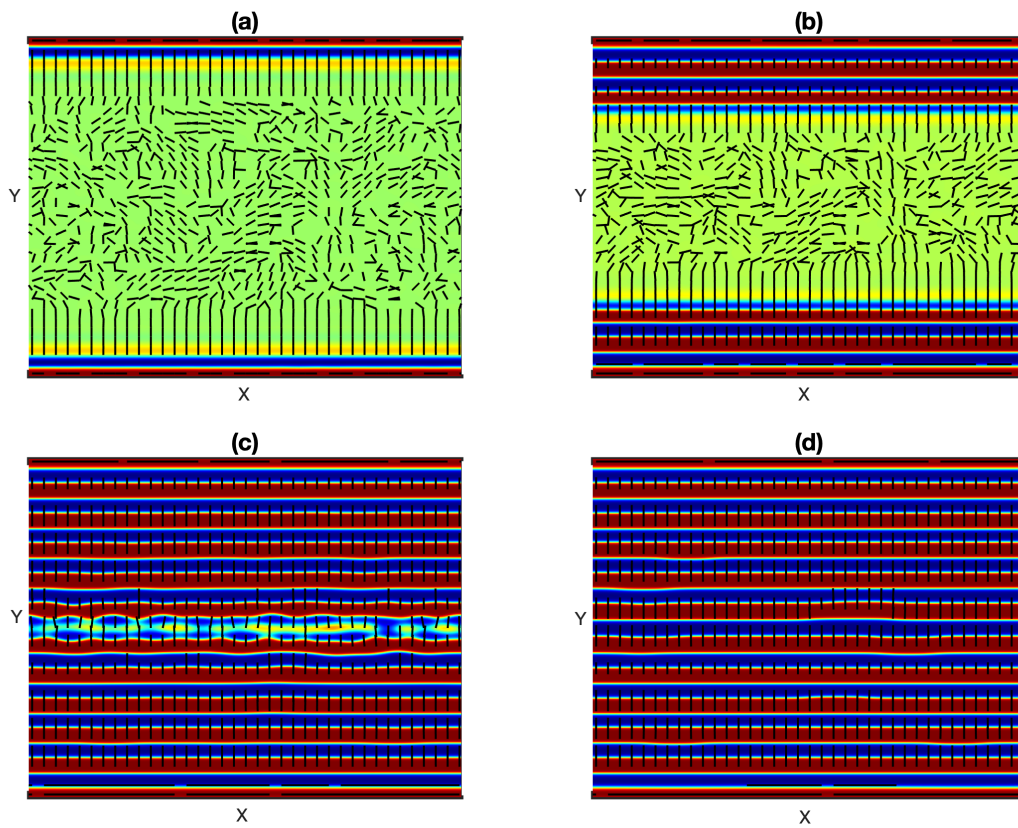
Figure 6: Time sequence of the polymer volume fraction ϕ and the subsampled director field for the phase separation of a polymer-LC mixture where the LC component is initially in isotropic state (thermotropic energy parameters $a = 80$, $B = -10$, $C = 160$) with homeotropic surface anchoring at (a) $t = 500$, (b) $t = 1500$, (c) $t = 3500$, (d) $t = 12000$. LC-rich phase is in red and polymer-rich phase is in blue.
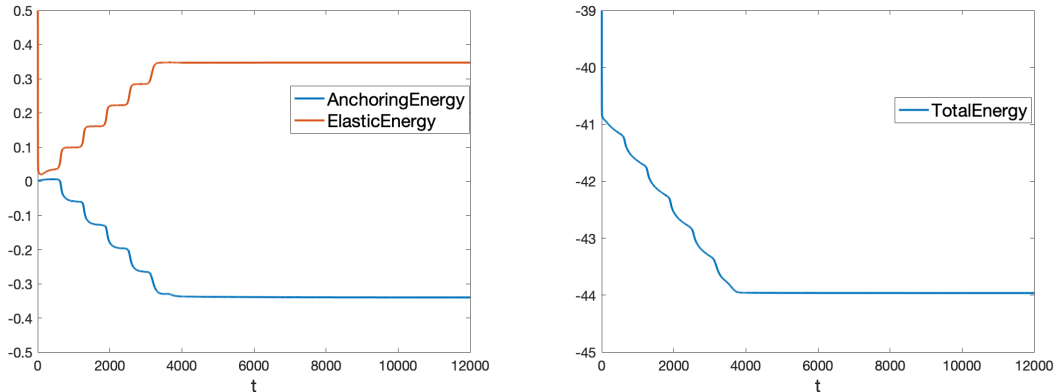
Figure 7: The anchoring energy and elastic energy (left) and total free energy (right) vs t for the lamellae structure formation.

lamellae growing from the walls inward, just as with homeotropic anchoring. However, the orientational field undergoes a very different distortion, with the orientational field aligning along the surface of the polymer-rich domains.

In the 3D channel, the phase separation and the formation of lamellae follows the same dynamics as the 2D case. Figure 9 presents isosurfaces of the polymer volume fraction and a subsampled director field at two different times for both wall anchoring aligned with the x axis and at a 45 degree angle between the x and z axis. The surface anchoring is homeotropic. As in the 2D case, once the phase-separated layers cover the entire channel, the system reaches an equilibrium and coarsening is arrested.

5 Conclusion

We have presented a numerical investigation, both in 2D and 3D, of the ordering and structure formation of a polymer nucleating in a LC continuous phase induced from temperature quenching. The polymer-LC system is confined between two parallel walls which are rubbed and coated to provide the strong planar long-range wall anchoring. Both homeotropic and planar surface anchoring are considered at the polymer-LC interface. The model is the Ginzburg-Landau theory for the conserved composition density ϕ, which represents the volume fraction of the polymer, and the non-conserved nematic tensor order parameter Q, which describes the orientation of the rigid rod-like nematic molecules. To our knowledge, this is the first 3D numerical investigation of nucleation in a confined geometry. Our study demonstrates that the presence of the nematic liquid crystal has profound effect on the morphology of nucleation of the minority phase. Moreover, the long-range wall anchoring and surface anchoring dramatically affect the orientation of the ordered structures. With certain set of parameters, remarkable polymer-rich domain chain structures are observed when quenching from the nematic initial state in
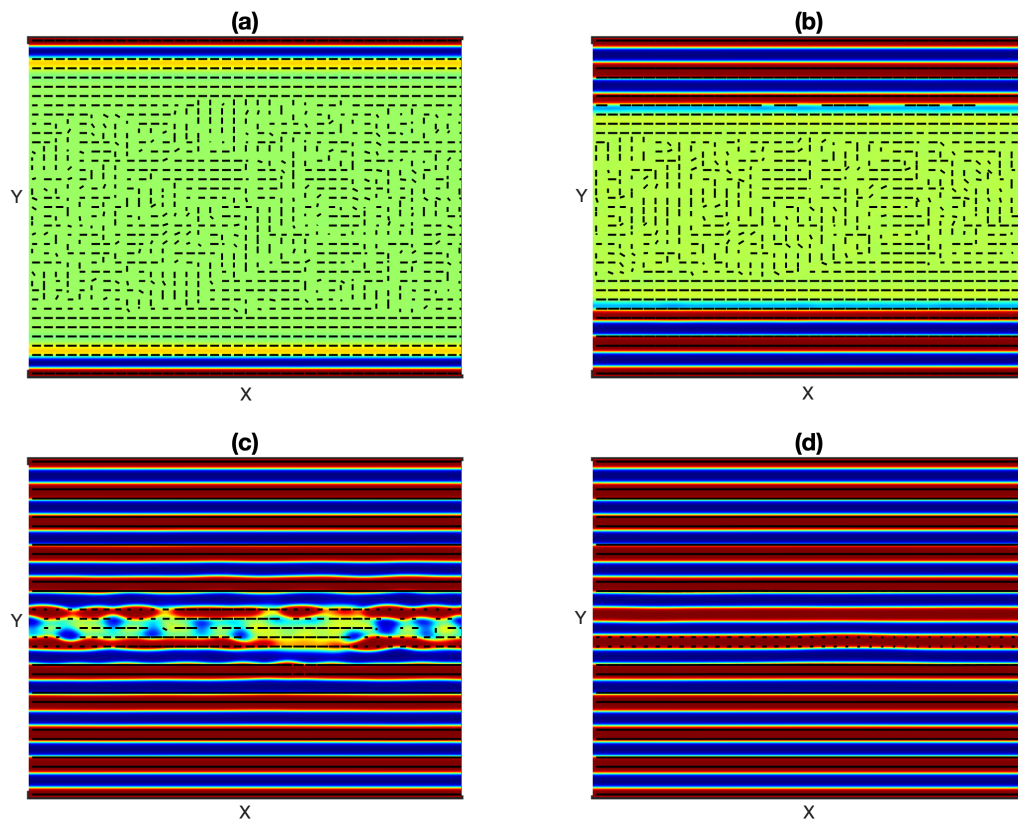
Figure 8: Time sequence of the polymer volume fraction ϕ and the subsampled director field for the phase separation of a polymer-LC mixture where the LC component is initially in isotropic state (thermotropic energy parameters $a = 80$, $B = -10$, $C = 160$) with planar surface anchoring at (a) $t = 500$, (b) $t = 1500$, (c) $t = 3500$, (d) $t = 12000$. LC-rich phase is in red and polymer-rich phase is in blue.
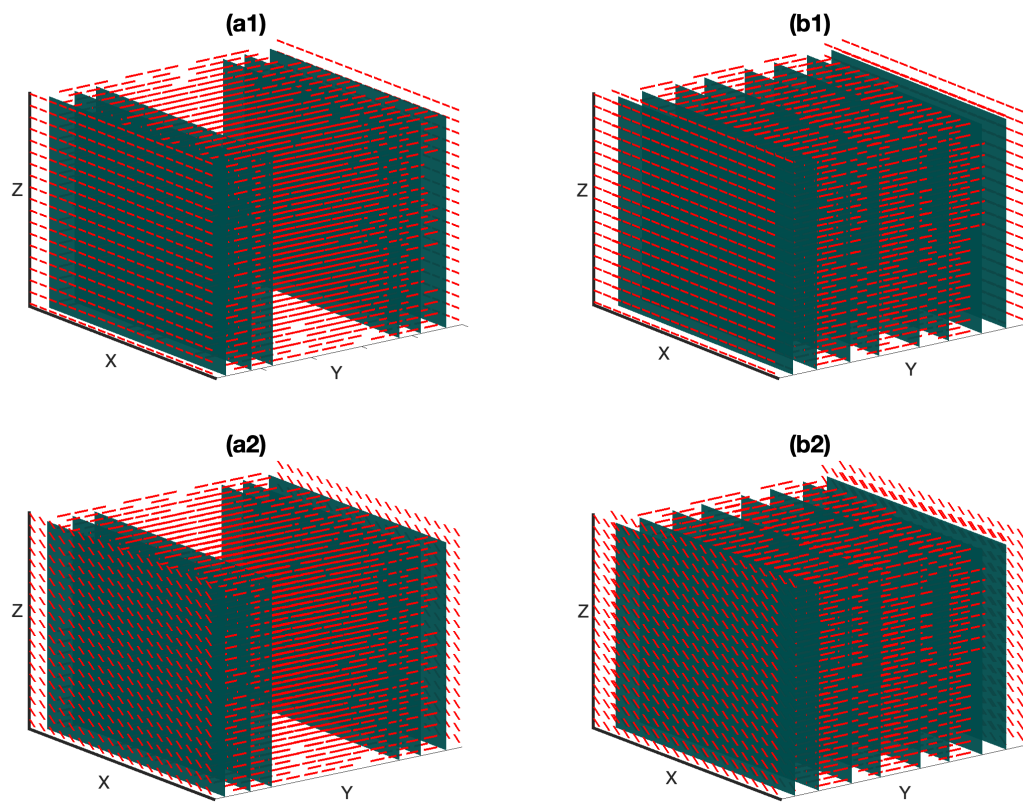
Figure 9: The top (bottom) two plots show isosurfaces of ϕ and a sample of the director field at $t = 500$ (left) and $t = 3500$ (right) when the wall anchoring is along the x axis (top) and at a 45 degree angle (bottom). The surface anchoring is homeotropic and the thermotropic energy parameters are $a = 80$, $B = -10$, $C = 160$.

both the 2D and 3D channel. However, there is no apparent mechanism in this Landau-de Gennes model to arrest the coarsening of the polymer-rich domains and eventually the chain structure order is destroyed. As argued in [32], the highly ordered array of monodisperse droplet chains observed in experiments is preserved and stable during phase separation because of dipole orientational defects formed in between the droplets. However, we show with a numerical example that dipole defects cannot be sustained in the Landau-de Gennes model and open up to two $-1/2$ point defects. The use of variable mobility that depends on both Q and ϕ might provide a mechanism to arrest or slow down the coarsening once the ordered structures have formed.

We also find a stable lamellae order when quenching from isotropic phase. The system reaches equilibrium with alternating polymer-rich and LC-rich layers, and the coarsening is arrested. While the model considered here has limitations, the results reveal the strong effects that the orientational order induced by the presence of a liquid crystal component and by anchoring can have on nucleation and phase separation, and underlines a potential mechanism for controlling morphology in this type of binary systems.

Acknowledgments

References

[1] P. D. Gennes, *The physics of liquid crystals*. Oxford, Clarendon Press, 1974.

[2] M.Mata, C.J.García-Cervera, and H. D. Ceniceros, *Ordering kinetics of a conserved binary mixture with a nematic liquid crystal component*, J. Non-Newtonian Fluid Mech. **212** (2014) 18–27.

[3] R. Nós, A. Roma, C. García-Cervera, and H. Ceniceros, *Three-dimensional coarsening dynamics of a conserved, nematic liquid crystal-isotropic fluid mixture*, J. Non-Newtonian Fluid Mech. **248** (2017) 62–73.

[4] M. Motoyama, H. Nakazawa, T. Ohta, T. Fujisawa, H. Nakada, M. Hayashi, and M. Aizawa, *Phase separation of liquid crystal-polymer mixtures*, Comput. Theor. Polym. Sci. **10** (2000), no. 3-4 287–297.

[5] H. Nakazawaa, S. Fujinami, M. Motoyama, T. Ohta, T. Araki, H. Tanaka, T. Fujisawa, H. Nakada, M. Hayashi, and M. Aizawa, *Phase separation and gelation of polymer-dispersed liquid crystals*, Comput. Theor. Polym. Sci. **11** (2001), no. 6 445458.

[6] J. Xia, J. Wang, Z. Lin, F. Qiu, and Y. Yang, *Phase separation kinetics of polymer dispersed liquid crystals confined between two parallel walls*, Macromolecules **39** (2006), no. 6 2247–2253.

[7] Y. J. Jeon, Y. Bingzhu, J. Rhee, D. Cheung, and M. Jamil, *Application and new developments in polymer-dispersed liquid crystal simulation studies*, Macromol. Theory Simul **16** (2007), no. 7 643–659.

[8] A. Matsuyama and R. Hirashima, *Phase separations in liquid crystal colloid mixtures*, J. Chem. Phys. **128** (2008), no. 4 044907.

[9] S. Bronnikov, S. Kostromin, and V. Zuev, *Thermally induced isotropic-nematic phase separation in mixtures of low-molecular weight and polymer liquid crystals, Soft Mater.* **11** (2013), no. 1 6–12.

[10] S. Bronnikov, C. Racles, and V. Cozan, *Kinetics of the nematic phase growth across the isotropic-nematic phase transition in polymerdispersed liquid crystals, Liq. Cryst.* **36** (2009), no. 3 319–328.

[11] C. Muratova and W. E, *Theory of phase separation kinetics in polymerliquid crystal systems, J. Chem. Phys.* **116** (2002), no. 11 4723.

[12] E. Soulé, N. Abukhdeir, and A. Rey, *Thermodynamics, transition dynamics, and texturing in Polymer-Dispersed Liquid Crystals with Mesogens exhibiting a direct isotropic/smectic-A transition, Macromolecules* **42** (2009), no. 24 94869497.

[13] A. Lapena, S. Glotzer, S. Langer, and A. Liu, *Effect of ordering on spinodal decomposition of liquid-crystal/polymer mixtures, Phys. Rev. E* **60** (1999), no. 1 R29.

[14] E. Soulé and A.D.Rey, *Modelling complex liquid crystal mixtures: from polymer dispersed mesophase to nematic nanocolloids, Phys. Rev. Lett.* **112** (2014), no. 22 225501.

[15] A. Matsuyama, *Nematic Ordering in Mixtures of Polymers and Liquid Crystals, Res. Rep. Fac. Eng. Mie Univ.* **27** (2002) 9–22.

[16] A. Bray, *Theory of phase-ordering kinetics, Adv. Phys.* **43** (1994), no. 3 357–459.

[17] A. Bray, *Coarsening dynamics of phase-separating systems, Philos. Trans. R. Soc., A* **361** (2004), no. 1805 781–792.

[18] P. Drzaic, *Liquid Crystal Dispersions*, vol. 1. World Scientific: Singapore, 1995.

[19] P. Drzaic, *Putting liquid crystal droplets to work: a short history of polymer dispersed liquid crystals, Liq. Cryst.* **33** (2006), no. 11-12 12811296.

[20] J. Lyu, H. Kikuchi, D. Kim, J. Lee, K. Kim, H. Higuchi, and S. Lee, *Phase separation of monomer in liquid crystal mixtures and surface morphology in polymer-stabilized vertical alignment liquid crystal displays, J. Phys. D: Appl. Phys.* **44** (2011), no. 32 325104.

[21] F. Ahmad, M. Jamil, L. Woo, and Y. Jeon, *The investigation of molecular affinity involved in poly(ethylene glycol)-based polymer-dispersed liquid crystal display, Colloid Polym. Sci.* **290** (2012), no. 7 599606.

[22] H. Kakiuchida, M. Tazawa, K. Yoshimura, and A. Ogiwara, *Optical diffractometry of highly anisotropic holographic gratings formed by liquid crystal and polymer phase separation, Phys. Rev. E* **86** (2012), no. 6-1 061701.

[23] R. Shanks and D. Staszczyk, *Thermal and optical characterization of polymerdispersed liquid crystals, Int. J. Polym. Anal.* **2012** (2012) 767581.

[24] J.-D. Cho, S.-S. Lee, S.-C. Park, Y.-B. Kim, and J.-W. Hong, *Optimization of LC droplet size and electro-optical properties of acrylate-based polymer-dispersed liquid crystal by controlling photocure rate, J. Appl. Polym. Sci.* **130** (2013), no. 5 30983104.

[25] R. Deshmukh and M. Malik, *Effect of dichroic dye on phase separation kinetics and electro-optical characteristics of polymer dispersed liquid crystals, J. Phys. Chem. Solids* **74** (2013), no. 2 215224.

[26] M. Ellahi, F. Liu, P. Song, Y. Gao, H. Cao, M. Rafique, M. Khaskheli, M. Z. Iqbal, and H. Yang, *Influence of the multi-functional epoxy monomers structure on the electro-optical properties and morphology of polymer-dispersed liquid crystal films, Polym. Bull.* **70** (2013), no. 11 29672980.

[27] J.-H. Lee and T.-H. Yoon, *Effect of the surface affinity of liquid crystals and monomers on the orientation of polymer-dispersed liquid crystal, Jpn. J. Appl. Phys.* **52** (2013), no. 9R 091702.

[28] S.-L. Hou, W.-K. Choi, and G.-D. Su, *Ultra-bright heads-up displays using a method of projected color images by combination of LEDs and polymer-dispersed liquid crystals, J. Disp. Technol.* **10** (2014) 228234.

[29] P. Yue, J. Feng, C. Liu, and J. Shen, *A diffuse-interface method for simulating two-phase flows of complex fluids*, *J. Fluid Mech.* **515** (2004) 293317.

[30] P. Hohenberg and B. Halperin, *Theory of dynamic critical phenomena*, *ReV. Mod. Phys.* **49** (1977) 435.

[31] A. Liu and G. F. Fredrickson, *Phase Separation Kinetics of Rod/Coil Mixtures*, *Macromolecules* **29** (1996) 8000.

[32] J.-C. Loudet, P. Barois, and P. Poulin, *Colloidal ordering from phase separation in a liquid-crystalline continuous phase*, *Nature* (2000), no. 407 611613.

[33] P. Poulin, H. Stark, T. Lubenski, and D. Weitz, *Novel colloidal interactions in anisotropic fluids*, *Science* **275** (1997), no. 5307 1770–1773.

[34] N. Silvestre, Q. Liu, B. Senyuk, I. Salyukh, and M. Tasinkevych, *Towards template-assisted assembly of nematic colloids*, *Phys. Rev. Lett.* **112** (2014), no. 22 225501.

[35] H. Stark, *Physics of colloidal dispersions in nematic liquid crystals*, *Phys. Rep.* **351** (2001), no. 6 387–474.

[36] J. Loudet, P. Barois, P. Auroy, P. Keller, H. Richard, and P. Poulin, *Colloidal Structures from Bulk Demixing in Liquid Crystals*, *Langmuir* **20** (2004), no. 26 11336–11347.

[37] R. Trivedi, M. Tasinkevych, and I. Smalyukh1, *Nonsingular defects and self-assembly of colloidal particles in cholesteric liquid crystals*, *Phys. Rev. E* **94** (2016) 062703.

[38] C. Zhou, P. Yue, and J. Feng, *Dynamic Simulation of Droplet Interaction and Self-Assembly in a Nematic Liquid Crystal*, *Langmuir* **24** (2008), no. 7 3099–3110.

[39] T. Porenta, S. Copar, P. Ackerman, M. Pandey, M. Varney, I.I.Smalyukh, and S. umer, *Topological switching and orbiting dynamics of colloidal spheres dressed with chiral nematic solitons*, *Sci. Rep.* **4** (2014) 7337.

[40] B. Senyuk, Q. Liu, S. He, R. Kamien, R. Kusner, T. Lubensky, and I. Smalyukh, *Topological colloids*, *Nature* **493** (2013), no. 7431 200205.

[41] S. Alama, L. Bronsard, and X. Lamy, *Minimizers of the Landau-de Gennes energy around a spherical colloid particle*, *Arch. Rational Mech. Anal.* **222** (2016), no. 1 427450.

[42] M. Ravnik and S. Zumer, *Landaude Gennes modelling of nematic liquid crystal colloids*, *Liq. Cryst.* **36** (2009), no. 10-11 12011214.

[43] F. Lin and C. Liu, *Static and dynamic theories of liquid crystals*, *J. Partial Differ. Equ.* **14** (2001), no. 4 289–330.

[44] S. Mkaddem and E. C. Gartland, *Fine structure of defects in radial nematic droplets*, *Phys. Rev. E* **62** (2000) 6694 6705.

[45] A. Majumdar and A. Zarnescu, *Landau-De Gennes theory of nematic liquid crystals: the Oseen-Frank limit and beyond*, *Arch. Ration. Mech. Anal.* **196** (2010), no. 1 227280.

[46] P. Flory, *Thermodynamics of High Polymer Solutions*, *J. Chem. Phys.* **10** (1942) 51–61.

[47] M. Huggins, *Solutions of Long Chain Compounds*, *J. Chem. Phys.* **9** (1941) 440.

[48] V. Anderson, E. Terentjev, S. Meeker, J. Crain, and W. Poon, *Cellular solid behaviour of liquid crystal colloids 1: Phase separation and morphology*, *Eur. Phys. J. E* **4** (2001) 11–20.

[49] K. Schiele and S. Trimper, *On the Elastic Constants of a Nematic Liquid Crystal*, *Phys. Status Solidi B* **118** (1983) 267274.

[50] V. Badalassi, H. Ceniceros, and S. Banerjee, *Computation of multiphase systems with phase field models*, *J. Comput. Phys.* **190** (2003), no. 2 371–397.

[51] G. Krausch, E. K. C. Dia, J. Marko, and F. Bates, *nterference of spinodal waves in thin polymer films*, *Macromolecules* **26** (1993), no. 21 5566–5571.

[52] G. Brown and A. Chakrabarti, *Ordering of block copolymer melts in confined geometry*, *Chem. Phys.* **102** (1995), no. 3 1440–1448.